
Article:
Jiang, L, Wang, S, Xie, Y et al. (2022) Decoupled Fractional Super-Twisting Stabilization of Interconnected Mobile Robot Under Harsh Terrain Conditions. IEEE Transactions on Industrial Electronics, 69 (8). pp. 8178-8189. ISSN: 0278-0046

https://doi.org/10.1109/tie.2021.3111557

Decoupled Fractional Super-Twisting Stabilization of Interconnected Mobile Robot Under Harsh Terrain Conditions

Liquan Jiang, Shuting Wang, Yuanlong Xie, *Member, IEEE,* Shengquan Xie, *Senior Member, IEEE*, Shiqi Zheng, *Member, IEEE*, Jie Meng, Han Ding, *Senior Member*

***Abstract*—The four-wheel omnidirectional mobile robot usually suffers disturbed or unstable lateral motion under harsh terrain conditions (such as uneven or oiled ground). Generally for such a challenging situation, the lumped disturbances and interconnected states render available coupling solutions difficult to achieve demand-satisfied performance. This paper proposes a novel decoupled fractional super-twisting sliding mode control (FST-SMC) method by (*i*) constructing an inverse system-based decoupling to form a pseudolinear composition system; (*ii*) presenting an enhanced nominal sliding law for chattering mitigation and (*iii*) designing an unbiased multi-layer fuzzy estimator with gain-learning capacity to compensate for the lumped disturbances actively. Given that the identified disturbances can be directly reflected in the FST-SMC law, this method guarantees an accurate and robust control without causing gain overestimation. Theoretical analysis is offered to verify the asymptotic stability. Under harsh terrain conditions, experimental results validate the effectiveness of the proposed FST-SMC method.**

***Index Terms*—Mobile robot, super-twisting sliding mode control, lumped disturbance, interconnected state**

I. Introduction

DUE to higher efficiency and strengthened adaptability, autonomous mobile robots have become an indispensable part of the unmanned industry [1]. Compared with differential mobile robots, the four-wheel omnidirectional mobile robot (FOMR) actuated by in-wheel or hub motors can achieve better maneuverability for practical implementation [2]. Without changing the wheels' directions, a FOMR facilitates the main body of wheels and rollers to rotate actively, thus offering superior mobility for an efficient move arbitrarily. This brings the FOMR notable potential in industrial applications such as logistics and warehousing, therefore enabling retrofitting and renovatinzg of typical manufacturing plants. However, the wheel-terrain interaction of the concerned FOMR usually interferes with harsh ground conditions (such as the oiled or bumped cover) [3]. Moreover, unknown disturbances and uncertainties inevitably exist (e.g., parametric perturbations or unmodeled dynamics) from the adaptive control context. This may lead to degraded system performance or even unstable dynamics such as wheel slip and lateral sway [4], [5]. Thus, how to ensure stable and accurate control of a FOMR must be resolved for harsh industrial scenarios.

Although a FOMR benefits from its independently driven and actuation features, capitalizing on the coordinated utilization of four distributed actuators to achieve fast and accurate torque scheduling for enhancing lateral stability is difficult [6]. In practice, the yaw rate and sideslip angle can be regarded as the universally applied indicators of system stability and dynamic performance, which considerably benefit the lateral motion control. Compared with anti-lock braking control and traction control, direct yaw moment control (DYMC) can compensate for the steering input with yaw moment generated by longitudinal tire force [7], [8]. DYMC helps specify dynamic capacities in terms of driving torque and steering and enhancing reliability and mobility [9], [10]. Apart from its merit of easy implementation, DYMC can accommodate the longitudinal-lateral motion of the FOMR in different scenarios [11]. However, for lateral control, the interconnected states (i.e., yaw rate and sideslip angle) imply that the concerned FOMR is a complex and strongly coupled multi-input multi-output (MIMO) system [12], [13]. The coupling or interconnection between the inputs and states of such a MIMO FOMR system results in difficulties to reach a given objective [14]. This would alleviate the robustness and stabilization superiority of DYMC solutions, leading to a dilemma for enhancing the accuracy and efficiency of a FOMR lateral motion control system concerned here.

Given that the interconnected states may worsen the lateral performances of the FOMR coupled studies, the decoupling control of FOMR deserves deep investigation [15]. Generally, decoupling allows to design a state independent controller by simplifying the system control framework and eliminating the interaction and interference of variables [16]. To date, a flotilla of explorations exists dedicated to this research area [17], [18]. An inverse technique is adopted to decouple a system with three inputs and three outputs to achieve a robust control [19], [20]. A proportional integral-based method is proposed to decouple the lateral velocity and yaw rate of a four-wheel vehicle [21]. Among existing decoupling works, the differential geometry method transforms the control problem into the geometric domain, which involves complex coordinate transformation. In comparison, the inverse system-based one is more intuitive and easier to understand [22]. We can construct the inverse system and cascade it with the original system to realize decoupling. Thus, the original MIMO systems with

The work was funded by National Natural Science Foundation of China under Grant 52105019, and Guangdong Basic and Applied Basic Research Foundation under Grant 2020A1515110464 (*Corresponding author: Y. L. Xie*)

L. Jiang, S. Wang, Y. Xie, J. Meng, and H. Ding are with the School of Mechanical Science and Engineering, Huazhong University of Science and Technology, Wuhan, China (email: hustlqj@hust.edu.cn; wangst@hust.edu.cn; yuanlongxie@hust.edu.cn; mengjie_10@hust.edu.cn; dinghan@hust.edu.cn).

S. Zheng is with the School of Automation, China University of Geosciences, Wuhan 430074, China ((e-mail: zhengshiqi@cug.edu.cn).

S. Xie is with the School of Electronic and Electrical Engineering, University of Leeds, Leeds, LS2 9JT, UK, in collaboration with the Institute of Rehabilitation Engineering, Binzhou Medical University, Yantai 264033, China (e-mail: S.Q.Xie@leeds.ac.uk).

interconnected states can be decomposed into several single-input single-output subsystems. This brings advantages and convenience for the controller design of each subsystem [23], [24]. For a system that can be pseudo linearized and decoupled using inverse system theory, the accurate analytical model is a prerequisite. However, precisely identifying the accurate structure and parameters of an industrial system is difficult, especially for a complex system, such as the FOMR [25], [26]. Hence, achieving the purpose of decoupling control is difficult by only utilizing the inverse system idea, and the necessary model estimation often renders the decoupling system to operate in a nonideal condition given that it may mitigate the robustness and convergence [27]. In this sense, the inevitable disturbances or structural uncertainties resulted from nonideal modeling or linearization should be well handled when deriving a decoupled tracking controller. For lateral control of the FOMR, a practical method must also address the lumped disturbances caused by harsh wheel-terrain interactions (such as uneven or oiled ground). *Ultimately, the anti-disturbance robust control relating to decoupling lateral stabilization of the FOMR must be investigated, which motivates this research.*

When it comes to robust control, sliding mode control (SMC) has control superiors in disturbance alleviation and dynamic tracking [28], [29]. This method can drive the resultant trajectory into a bounded switching region and maintaining it therein for subsequent periods [30]. To ensure state convergence, the control gains of SMC solutions normally must satisfy specific conditions relating to the upper boundaries or the derivatives of the lumped disturbances. For instance, in [31], a super-twisting SMC method was used to handle the unknown disturbances. However, the mentioned information may be unavailable in the industrial environment. Especially, the considered FOMR system often suffers nonideal terrain conditions such as oiled, damaged or bumped grounds, implying large and time-varying disturbances or uncertainties. Another major drawback is that relative high control gains should be selected in principle to ensure the system's robustness. Such a passive anti-disturbance manner may lead to gain overestimation or even serious chattering phenomena. The scheduling of high gain imposes a tradeoff between dynamic tracking and disturbance attenuation [32]-[34]. Given this context, guaranteeing a sufficiently high- performance control for the FOMR system is extremely difficult, which is a nonlinear, and strongly coupling system with the time-variance of parameters as well as unavoidable disturbances.

Consequently, to achieve effective asymptotic stabilization control, this paper proposes a fuzzy fractional super-twisting SMC (FST-SMC) for the interconnected FOMR system. The presented method can distinctly handle the decoupled lateral motion control and disturbance rejection of the considered FOMR system. The contributions are summarized as follows.

1) An inverse system-based decoupling scheme is presented to decompose the original MIMO FOMR system into several single-input single-output subsystems. Such a pseudo linearization is beneficial for intuitively and immensely simplifying the decoupled controller design and stability analysis of complex interconnected systems.
2) A modified FST-SMC is proposed to ensure that each subsystem is driven into the constructed sliding manifold. Different from the traditional SMC schemes [31], [35], a new fractional super-twisting switching law is designed to mitigate the undesirable chattering without acquiring the upper boundary of the disturbances or related derivatives. Therefore, the gain overestimation can be well addressed.
3) Unlike the traditional decoupling control scheme [23], the active anti-disturbances reduction is realized for the decoupled FOMR system. Considering the characteristics of the pseudo linearized system, a multi-layer fuzzy neural network (MFNN) is designed to adaptively predict and compensate for the lumped disturbances. This can enhance the control robustness given that the estimated disturbances are utilized directly in the control law.
4) By combining Lyapunov theory, sufficient conditions of learning parameters and control gains are derived for the decoupling of FST-SMC dynamics with guaranteed asymptotic convergence and closed-loop stability.

The remainder of the paper is constructed as follows. Section II provides the system modeling and problem statement. Section III proposed the designed decoupled FST-SMC stabilization framework. Thereafter, Section IV presents the experimental validations. Conclusions are offered in Section V.

Notations: Throughout this paper, $\mathbb{R}^n$ represents the n dimensional Euclidean space. diag{...} is the block diagonal matrix. $\lambda_{\min}(\mathrm{A})$ and $\lambda_{\max}(\mathrm{A})$ represent the largest and the smallest eigenvalue of matrix A , respectively. The notation $\lfloor s \rceil^{\alpha}$ is used to represent $|s|^{\alpha}\,sign(s)$ with $sign(s)$ denoting the set-valued function equal to its *sign* if $s \neq 0$.

II. Dynamical Modeling and Problem Statement

A. Lateral Dynamical Modeling

The lateral dynamic model of the concerned FOMR system is a nonlinear MIMO system with interconnected states. In the yaw plane, the four-wheel dynamics are denoted as [31]

$$mv_x\dot{\beta} = \sum_{i=1}^{2}(F_{xi}\sin\delta_i + F_{yi}\cos\delta_i) - \sum_{i=3}^{4}(F_{xi}\sin\delta_i - F_{yi}\cos\delta_i) - \gamma + d_1 \quad (1)$$

$$I_z\dot{\gamma} = l_f\sum_{i=1}^{2}(F_{xi}\sin\delta_i + F_{yi}\cos\delta_i) + l_r\sum_{i=3}^{4}(F_{xi}\sin\delta_i - F_{yi}\cos\delta_i) + M_\omega + d_2 \quad (2)$$

$$M_\omega = 0.5d(F_{fx} - F_{fy})\cos\delta_f + 0.5d(F_{rx} - F_{ry})\cos\delta_r \quad (3)$$

where m is the total mass, I_z is the inertia moment through the center of gravity (CG), β and γ denote the sideslip angle and yaw rate, separately, F_{xi} and F_{yi} are the longitudinal and lateral tire force of ith tire, respectively, δ_f and δ_r are the virtual front and rear wheel angles, separately, $d_{i=1,2}$ are the lumped disturbances, M_ω is the yaw moment of inertia generated by the traction moment of four wheels, l_f and l_r are the distances between the front and rear axles and the CG, separately, $F_{fi=x,y}$ and $F_{ri=x,y}$ are the virtual wheel forces shown in Fig. 1, $\delta_{i=1,2,3,4}$ are the steer angles, and v_x denotes the longitude velocity.

As demonstrated in Fig. 1, the single-track model of FOMR can be formulated using the front and rear virtual wheels, i.e.,

$$mv_x\dot{\beta} = F_{fy}\cos\delta_f + F_{ry}\cos\delta_r - \gamma + d_1 \quad (4)$$

$$I_z\dot{\gamma} = l_fF_{fy}\cos\delta_f - l_rF_{ry}\cos\delta_r + M_\omega + d_2 \quad (5)$$

With the slip ratio and stiffness coefficient, the relationship between the tie force and steering angles can be approximated under a small steering angle (i.e., $\cos\sigma_f = 1$ and $\sin\sigma_f = \sigma_f$)

$$F_{xi} = c_ir_s,\ \ r_s = (RW - v_x)\max^{-1}(RW, v_x),\ i = r, f \quad (6)$$

$$F_{yf} = -2c_f(\beta + \gamma l_f v_x^{-1} - \delta_f),\ F_{yr} = -2c_r(\beta - \gamma l_f v_x^{-1} + \delta_r) \quad (7)$$

where r_s denotes the slip ratio, R denotes the wheel radius, c_f and c_r are the stiffness coefficients of front and rear wheels,

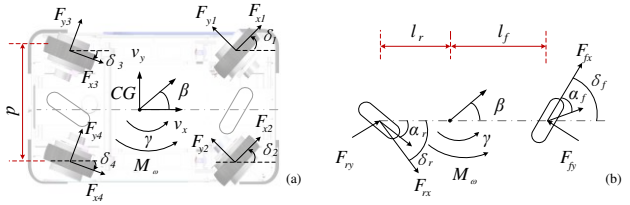

Fig. 1 FOMR System modeling. (a) Four-wheel model; (b) Single-track model.

respectively, and W is the angular velocity.

To simplify the lateral control model, we define the proportional relationship between the front and rear wheels as $\delta_r = k\delta_f$ with k being a pre-defined parameter. Then, the re-defined state model can be obtained as

$$\dot{x} = Ax + Bu + d \tag{8}$$

where $x = (\beta, \gamma)^{\mathrm{T}}$ is the state vector, $u = (\delta_f, M_\omega)^{\mathrm{T}}$ denotes the control input vector, $d = [d_1 \quad d_2]^{\mathrm{T}}$ denotes the lumped disturbance, and the system parametric vectors are expressed by

$$A = \begin{bmatrix} -2(c_f + c_r)/(mv_x) & 2(c_r l_r - c_f l_f)/(mv_x^2) - 1 \\ 2(c_r l_r - c_f l_f)/I_z & -2(c_r l_r^2 - c_f l_f^2)/(I_z v_x) \end{bmatrix},$$

$$B = \begin{bmatrix} 2(kc_f - c_r)/(mv_x) & 2(kc_r l_r + c_f l_f)/I_z \\ 0 & 1/I_z \end{bmatrix}^{\mathrm{T}}$$

B. Problem Formulation

Generally, given that the interconnected yaw rate and sideslip angle are more sensitive to the system stability under lateral motion framework, these states are considered as the key control performance indicators of the FOMR. Then, the dynamic control problem of the FOMR concerned here is transferred as the DYMC issue to achieve robust stabilization control. Consequently, the objective of this paper is to propose a decoupled FST-SMC method that will make the DYMC output states accurately track the desired trajectories (or a constructed reference model [31]). This will be realized by designing (*i*) an inverse-system decoupling scheme to achieve a pseudo linear composition system; and (*ii*) an FST-SMC law to address the active anti-disturbance issue of the decoupled FOMR system. Through this, the explored method can simultaneously enhance the disturbance suppression and trajectory tracking capacities of the concerned FOMR system.

III. Main Results

A. FST-SMC Design

Given that the lumped disturbances may cause unstable oscillations, a novel FST-SMC law is proposed to specify the nominal tracking performance of the independent subsystems. First, inverse system theory is utilized to decouple the original MIMO system as several independent subsystems. The existence of the inverse system, i.e., the invertibility, should be ensured by the system derivative order. To this end, the FOMR system with the states and output signals are expressed as

$$\dot{x}_1 = f_1(x,u),\ \dot{x}_2 = f_2(x,u), \cdots,\ \dot{x}_n = f_n(x,u) \tag{9}$$

$$\dot{y}_1 = h_1(x,u),\ \dot{y}_2 = h_2(x,u),\ \cdots, \dot{y}_g = h_g(x,u) \tag{10}$$

where $x = (x_1, x_2, ..., x_n)^{\mathrm{T}} \in \mathbb{R}^n$ is the system state vector with n being the dimension, $u = (u_1, u_2, ..., u_j)^{\mathrm{T}} \in \mathbb{R}^j$ is the input vector with dimension j, and g is the dimension of y.

Further, one can simplify the FOMR system as

$$\dot{x} = f(x,u),\ y = h(x,u),\ x(t_0) = x_0 \tag{11}$$

where $y = (y_1, y_2, \ldots, y_g)^{\mathrm{T}} \in \mathbb{R}^g$ denotes the output vector, $f = (f_1, f_2, \ldots, f_n)^{\mathrm{T}}$ and $h = (h_1, h_2, \ldots, h_g)^{\mathrm{T}}$ are the parameter vectors, t_0 and x_0 are the initial time and state, respectively.

To ensure the reversibility of the FOMR system, the $\tilde{\alpha}$- order derivatives of y must be identified

$$y^{\tilde{\alpha}} = \partial y / \partial u^{\mathrm{T}} = [y_1^{(\alpha_1)}(x,u), y_2^{(\alpha_2)}(x,u), ..., y_g^{(\alpha_g)}(x,u)]^{\mathrm{T}} \tag{12}$$

where $\tilde{\alpha} = [\alpha_1, \alpha_2, \cdots, \alpha_g]^{\mathrm{T}}$ denotes the order vector.

By continuously computing the derivatives of y, a linear inverse system (i.e., a decoupled model) is finally achieved, implying that y can be expressed linearly with u. Then, the existence of the desired inverse system is judged by evaluating $\sum \tilde{\alpha} = \sum_{i=1}^{g} \alpha_i \le n$. Through the above steps, if the explicit control input u can be expressed as $\tilde{\alpha}$ -order derivatives of the output y, then an interconnected MIMO system can be decoupled as a reformulated inverse system.

For the concerned FOMR, as a typical MIMO system, the first order derivative of y is obtained

$$y^{(\tilde{\alpha})} = \begin{bmatrix} \beta^{(\alpha_1)} \\ \gamma^{(\alpha_2)} \end{bmatrix} = \begin{bmatrix} \dot{\beta} \\ \dot{\gamma} \end{bmatrix} = \begin{bmatrix} (F_{fy} + F_{ry})/(mv_x) - \gamma \\ (l_f F_{yf} - l_r F_{yr})/I_z + M_z/I_z \end{bmatrix}$$

$$= \begin{bmatrix} \dfrac{2(c_f + kc_r)}{mv_x} & 0 \\ 2\dfrac{c_f l_f - kc_r l_r}{I_z} & \dfrac{1}{I_z} \end{bmatrix} \begin{bmatrix} \delta_f \\ M_z \end{bmatrix} + \begin{bmatrix} -2\dfrac{c_f + kc_r}{mv_x}\beta + \dfrac{2c_r l_r - 2c_f l_f}{mv_x^2}\gamma \\ -2\dfrac{c_f l_f - c_r l_r}{I_z}\beta - 2\dfrac{c_f l_f^2 + crl_r^2}{I_z v_x}\gamma \end{bmatrix}$$

After the calculation of the first-order derivative of y, the linear expression of the control variable can be realized. Given that the derivative vector $\tilde{\alpha}$ satisfies $\tilde{\alpha} = [\alpha_1 \quad \alpha_2] = [1 \quad 1]$, the rank of the $y^{\tilde{\alpha}} = [y^{\alpha_1} \quad y^{\alpha_2}]$ is

$$M = rank\left[\frac{\partial y}{\partial u^{\mathrm{T}}}\right] = rank\begin{bmatrix} \dfrac{\partial \beta^{\alpha_1}}{\partial \delta_f} & \dfrac{\partial \beta^{\alpha_1}}{\partial M_\omega} \\ \dfrac{\partial \gamma^{\alpha_2}}{\partial \delta_f} & \dfrac{\partial \gamma^{\alpha_2}}{\partial M_\omega} \end{bmatrix} = 2 \tag{13}$$

Considering that the rank of the $\partial y / \partial u^{\mathrm{T}}$ is equal to $\sum \tilde{\alpha} = \alpha_1 + \alpha_2 = 2$, there exists an inverse system that can be applied to decouple the lateral model of FOMR. Then, the control variable u can be expressed as the state variable y, thus the inverse system equation can be written as $u = \vartheta(x, y^{\tilde{\alpha}})$ with ϑ being the inverse system expression of formula. Under system uncertainties G, the decoupled system is determined by

$$u = \begin{bmatrix} u_1 \\ u_2 \end{bmatrix} = \begin{bmatrix} mv_x/(2(c_f + kc_r)) & 0 \\ 0 & I_z \end{bmatrix} \begin{bmatrix} \dot{y}_1 \\ \dot{y}_2 \end{bmatrix} + \psi + \mathrm{G} \tag{14}$$

$$\psi = -\begin{bmatrix} mv_x/(2(c_f + kc_r)) & 0 \\ mv_x(kl_r c_r + l_f c_f)/(kc_r - c_f) & I_z \end{bmatrix} A \begin{bmatrix} \beta \\ \gamma \end{bmatrix} + \begin{bmatrix} 0 \\ u_1 mv_x(kl_r c_r + l_f c_f)/(kc_r - c_f) \end{bmatrix} \tag{15}$$

Then, the output state and control values of the derived FOMR inverse system can be transferred as $\mathrm{X} = [u_1, u_2]^{\mathrm{T}} = [\delta_f, M_z]^{\mathrm{T}}$ and $\mathrm{U} = [\dot{y}_1, \dot{y}_2]^{\mathrm{T}} = [\dot{\beta}, \dot{\gamma}]^{\mathrm{T}}$, respectively. Through this, one can achieve a pseudo linearized mapping relation for the original lateral motion FOMR system, i.e.,

$$\dot{\mathrm{X}} = \mathrm{AX} + \mathrm{BU} + \mathrm{G},\ \mathrm{X}(t_0) = \mathrm{X}_0 \tag{16}$$

where X_0 is the initial state, A and B are the related vectors.

Thus, the following sliding mode surface is provided

$$s = e + \lambda e^{\eta_1/\eta_2} + \tau D^{\rho-1} e \tag{17}$$

where $s = [s_1, s_2]^{\mathrm{T}} \in \mathbb{R}^2$ is the designed sliding variable, η_1 and

η_2 are positive odd numbers satisfying $1<\eta_1/\eta_2<2$, $\lambda,\tau\in\mathbb{R}^{2\times 2}$ are positive matrixes, $e^{\eta_1/\eta_2}=[e_1^{\eta_1/\eta_2},e_2^{\eta_1/\eta_2}]^{\mathrm{T}}$ with e_1 and e_2 being the state errors, D denotes the fractional operator [36], and ρ is a pre-defined fractional order.

To achieve a superior nominal tracking controller for the interconnected FOMR, we provide:

Theorem 1: For the decoupled FOMR system, with the equivalent control law U_{eq} and super-twisting switching law U_{sw}, if the following fractional SMC law U_{FSMC} are employed

$$\mathrm{U}_{FSMC}=\mathrm{U}_{eq}+\mathrm{U}_{sw} \tag{18}$$

$$\mathrm{U}_{eq}=\mathrm{B}^{-1}[-(1+\lambda\eta_1\eta_2^{-1}e^{\eta_1/\eta_2-1})^{-1}\tau D^{\rho}e-\mathrm{AX}+\dot{\mathrm{X}}_r] \tag{19}$$

$$\mathrm{U}_{sw}=(\mathrm{B}+\mathrm{B}\lambda\eta_1\eta_2^{-1}e^{\eta_1/\eta_2-1})^{-1}(-\sigma_1\Omega_1-\sigma_2\Omega_2) \tag{20}$$

$$\Omega_1(s)=\zeta_1|s|^{\alpha}+\zeta_2|s|^{0.5} \tag{21}$$

$$\begin{aligned}\dot{\Omega}_2(s)&=\dot{\Omega}_1(s)\Omega_1(s)\\&=\zeta_1^2\alpha|s|^{2\alpha-1}+(0.5+\alpha)\zeta_1\zeta_2|s|^{\alpha-0.5}+0.5\zeta_2^2 sign(s)\end{aligned} \tag{22}$$

where $\zeta_{i=1,2}$ are positive constants, X_r is the reference state, $\alpha\in(0,1)$ is the fractional order, and $\sigma_{i=1,2}\in\mathbb{R}^{+}$ are the adaptive gains, then, there exists a range of values for σ_1, σ_2, such that the designed sliding manifold can be forced to zero within finite time and remains on it for the subsequent periods.

Proof: The time derivative of s is

$$\dot{s}=\dot{e}+\lambda\eta_1\eta_2^{-1}e^{\eta_1/\eta_2-1}\dot{e}+\tau D^{\rho}e,\ \dot{e}=\dot{\mathrm{X}}-\dot{\mathrm{X}}_r \tag{23}$$

A straightforward calculation leads to

$$\dot{s}=\underbrace{(1+\lambda\eta_1\eta_2^{-1}e^{\eta_1/\eta_2-1})}_{\Xi}(\mathrm{AX}+\mathrm{BU}-\dot{\mathrm{X}}_r)+\tau D^{\rho}e \tag{24}$$

Assuming that the unknown disturbances G can be replaced by an unbiased estimator $\hat{\mathrm{G}}$ (as demonstrated in Section III.B), the integration of (18)-(22) and (24) yields

$$\dot{s}=\Xi(\mathrm{AX}+\mathrm{B}(\mathrm{U}_{eq}+\mathrm{U}_{sw})-\dot{\mathrm{X}}_r)+\tau D^{\rho}e=-\sigma_1\Omega_1-\sigma_2\Omega_2 \tag{25}$$

Define a state vector $\mathrm{M}=[\mathrm{M}_{\sigma_1},\mathrm{M}_{\sigma_2}]^{\mathrm{T}}$ with $\mathrm{M}_{\sigma_1}=\Omega_1$ and $\mathrm{M}_{\sigma_2}=\sigma_2\Omega_2$. A Lyapunov function candidate is chosen as

$$V_1=\mathrm{M}^{\mathrm{T}}P\mathrm{M},\ P=\begin{bmatrix}\mathrm{P}+\mathrm{Q}^2 & -\mathrm{Q}\\ -\mathrm{Q} & 1\end{bmatrix} \tag{26}$$

where $\mathrm{P}>0$ and $\mathrm{Q}>0$ are arbitrary time-invariant constants.

Note that $\dot{\Omega}_2=\dot{\Omega}_1\Omega_1$, one achieves

$$\dot{\mathrm{M}}=\begin{bmatrix}\dot{\Omega}_1(-\sigma_1\Omega_1-\sigma_2\Omega_2)\\ -\sigma_2\Omega_2\end{bmatrix}=\dot{\Omega}_1\underbrace{\begin{bmatrix}-\sigma_1 & 1\\ -\sigma_2 & 0\end{bmatrix}}_{\mathrm{J}}\mathrm{M}=\dot{\Omega}_1\mathrm{J}\,\mathrm{M} \tag{27}$$

Thus, the derivative of the Lyapunov function is obtained

$$\dot{V}_1=\dot{\mathrm{M}}^{\mathrm{T}}P\mathrm{M}+\mathrm{M}^{\mathrm{T}}P\dot{\mathrm{M}}=\dot{\Omega}_1\mathrm{M}^{\mathrm{T}}(\mathrm{J}^{\mathrm{T}}P+P\mathrm{J})\mathrm{M}=-\dot{\Omega}_1\mathrm{M}^{\mathrm{T}}Q\mathrm{M} \tag{28}$$

$$Q=\begin{bmatrix}2\sigma_1(\mathrm{P}+\mathrm{Q}^2)-2\mathrm{Q}\sigma_2 & \sigma_2-\mathrm{P}-\mathrm{Q}^2-\mathrm{Q}\sigma_1\\ \sigma_2-\mathrm{P}-\mathrm{Q}^2-\mathrm{Q}\sigma_1 & 2\mathrm{Q}\end{bmatrix} \tag{29}$$

Choosing $\sigma_2=\mathrm{P}+\mathrm{Q}^2+\mathrm{Q}\sigma_1$ leads to

$$Q-diag\{\mathrm{Q},\mathrm{Q}\}=\begin{bmatrix}2\sigma_1(\mathrm{P}+\mathrm{Q}^2)-2\mathrm{Q}\sigma_2-\mathrm{Q} & 0\\ 0 & \mathrm{Q}\end{bmatrix} \tag{30}$$

With the aid of Algebraic Riccati Inequality [37] and a small positive constant $\grave{\mathrm{o}}$, one can select

$$\sigma_1\geq\grave{\mathrm{o}}+(2\mathrm{P})^{-1}(2\mathrm{QP}+2\mathrm{Q}^3+\mathrm{Q}) \tag{31}$$

that ensures $Q-diag\{\mathrm{Q},\mathrm{Q}\}$ being positive defined and

$$\dot{V}_1=-\dot{\Omega}_1\mathrm{M}^{\mathrm{T}}Q\mathrm{M}\leq-\mathrm{Q}\left(\frac{\alpha\zeta_1}{|s|^{1-\alpha}}+\frac{\zeta_2}{2s^{0.5}}\right)\mathrm{M}^{T}\mathrm{M} \tag{32}$$

Given that $\lambda_{\min}\{P\}\|\mathrm{M}\|_2^2\leq\mathrm{M}^{T}P\mathrm{M}\leq\lambda_{\max}\{P\}\|\mathrm{M}\|_2^2$, $1-\alpha\in(0,1)$ and $\|\mathrm{M}\|_2^2=\mathrm{M}_{\sigma_1}^2+\mathrm{M}_{\sigma_2}^2=\zeta_1^2|s|^{2\alpha}+2\zeta_1\zeta_2|s|^{\alpha+0.5}+\zeta_2^2 s+\sigma_2^2\Omega_2^2$, we get

$$\zeta_2|s|^{1-\alpha}\leq\|\mathrm{M}\|_2\leq V_1^{0.5}\lambda_{\min}^{-0.5}\{P\},\ \|\mathrm{M}\|_2\geq V_1^{0.5}\lambda_{\max}^{-0.5}\{P\} \tag{33}$$

Substituting (33) into (32) results in

$$\dot{V}_1\leq-\mathrm{Q}\left(\frac{\alpha\zeta_1}{|s|^{1-\alpha}}+\frac{\zeta_2}{2s^{0.5}}\right)\|\mathrm{M}\|_2^2\leq-\frac{(\alpha\zeta_1\zeta_2+0.5\mathrm{Q})\lambda_{\min}^{0.5}\{P\}}{\lambda_{\max}\{P\}}V_1^{0.5} \tag{34}$$

Note that (34) reveals that $\dot{V}_1\leq 0$, thus ensuring the closed-loop stability. With $\Upsilon(\zeta_1,\zeta_2)\triangleq(\alpha\zeta_1\zeta_2+0.5\mathrm{Q})\lambda_{\min}^{0.5}\{P\}\lambda_{\max}^{-1}\{P\}$, the solution of $\dot{v}=-\Upsilon(\zeta_1,\zeta_2)\,v^{0.5}$, $v(0)=v_0>0$ is determined by $v(t)=(v_0^{0.5}-0.5\Upsilon t)^2$. When $V(s_0)\leq v_0$, we have $V_1\leq v$. Specifically, the finite convergence time is

$$T=2\Upsilon^{-1}(\zeta_1,\zeta_2)V^{0.5}(s_0) \tag{35}$$

Thus, with suitable σ_1 and σ_2, the constructed s and $\dot{s}$ are driven to zero within a finite time. Here completes the proof. ■

The decoupled FST-SMC framework is depicted in Fig. 2. For the concerned FOMR system, the following composite control law, which comprises the fractional super-twisting SMC U_{FSMC} and the anti-disturbance MFNN-based estimated law U_{MFNN}, are constructed as

$$\mathrm{U}=\mathrm{U}_{FSMC}+\mathrm{U}_{MFNN},\ \mathrm{U}_{MFNN}=-\mathrm{B}^{-1}\hat{\mathrm{G}} \tag{36}$$

As the lump disturbances G cannot be measured or monitored directly in practice, we provide an MFNN solution to estimate $\hat{\mathrm{G}}$, thus implementing the proposed FST-SMC law.

B. Unbiased Fuzzy Disturbance Estimator

By adjusting the learning parameters, an unbiased fuzzy disturbance estimator is designed as

$$\hat{\mathrm{G}}=\hat{w}^{\mathrm{T}}\hat{r}(e,\hat{\varpi}_1,\hat{\varpi}_2,\hat{\varpi}_3,\hat{\varpi}_4,\hat{\varpi}_5) \tag{37}$$

where $\hat{w}$ is the weight, $\hat{r}$ denotes the output of the fuzzy rules, $\hat{\varpi}_{i=1,\ldots,5}$ denote the adaptive parameters adjusted online in the MFNN framework with being the base width $\hat{\varpi}_1$, $\hat{\varpi}_2$ being the center vector, $\hat{\varpi}_3$ and $\hat{\varpi}_4$ being the inner feedback gains, and $\hat{\varpi}_5$ being the outer feedback gain, e is the control error vector, serving as the input of the disturbance estimator.

We construct $\hat{\mathrm{G}}=w^{*\mathrm{T}}r^{*}+\chi$, where χ is the mapping error, and $r^{*}=r^{*}(e,\varpi_1^{*},\varpi_2^{*},\varpi_3^{*},\varpi_4^{*},\varpi_5^{*})$ and specially w^{*} and $\varpi_{i=1,\ldots,5}^{*}$ are the related optimal parameters. Thus, one can obtain the estimation error as

$$\begin{aligned}\mathrm{G}-\hat{\mathrm{G}}&=w^{*\mathrm{T}}r^{*}+\chi-\hat{w}^{\mathrm{T}}\hat{r}=w^{*\mathrm{T}}(\hat{r}+\tilde{r})+\chi-\hat{w}^{\mathrm{T}}\hat{r}\\&=\tilde{w}^{\mathrm{T}}\hat{r}+\tilde{w}^{\mathrm{T}}\tilde{r}+\hat{w}^{\mathrm{T}}\tilde{r}+\chi=\tilde{w}^{\mathrm{T}}\hat{r}+\tilde{w}^{\mathrm{T}}\tilde{r}+\chi_0\end{aligned} \tag{38}$$

where $\chi_0=\hat{w}^{T}\tilde{r}+\chi$ denotes the approximation error, $\tilde{\varpi}=\varpi^{*\mathrm{T}}-\hat{\varpi}^{\mathrm{T}}$ and $\tilde{r}=r^{*\mathrm{T}}-\hat{r}^{\mathrm{T}}$.

The gradient direction of r_k should be obtained to acquire the transformation law of the adaptive parameters. Considering that, $\tilde{r}$ is expressed using the Taylor expansion

$$\tilde{r}=\sum_{i=1}^{5}\frac{\partial\tilde{r}}{\partial\varpi_i}\Big|_{|\varpi_i=\hat{\varpi}_i}(\varpi_i^{*}-\hat{\varpi}_i)+\chi_h=\sum_{i=1}^{5}dr_{\varpi_i}\tilde{\varpi}_i+\chi_h \tag{39}$$

where χ_h denotes the higher order term, and $dr_{\varpi_{i=1,\ldots,5}}$ are the coefficient matrices of the gradient vector, i.e.,

$$dr_{\varpi_i}=\left[\frac{\partial\tilde{r}_1^{\mathrm{T}}}{\partial\varpi_i},\frac{\partial\tilde{r}_2^{\mathrm{T}}}{\partial\varpi_i},\ldots,\frac{\partial\tilde{r}_k^{\mathrm{T}}}{\partial\varpi_i}\right]^{\mathrm{T}}\Big|_{\varpi_i=\hat{\varpi}_i} \tag{40}$$

The combination of (38) and (39) yields

$$\mathrm{G}-\hat{\mathrm{G}}=\tilde{w}^{\mathrm{T}}\hat{r}+\hat{w}^{\mathrm{T}}\sum_{i=1}^{5}\partial r_{\varpi_i}\cdot\tilde{\varpi}_i+\chi_m \tag{41}$$

where $\chi_m=\hat{w}^{\mathrm{T}}\chi_h+\chi_0$ denotes the sum of the approximation error, and assume that the differential of χ_m is limited by a

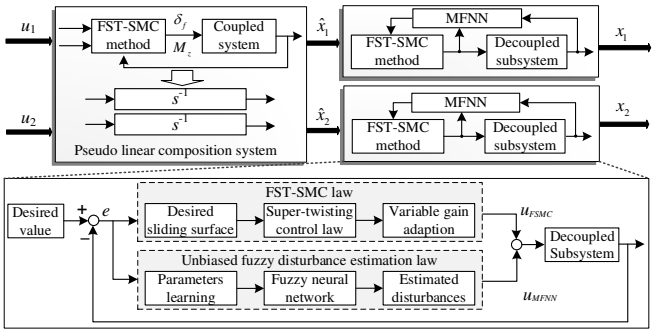

Fig. 2 Control framework of the proposed method

positive constant χ_d, i.e., $|\dot{\chi}_m| \le \chi_d$.

As shown in Fig. 3, the constructed MLNN contains the input, hidden, and output layers. The fuzzification and rule formulation are implemented in the hidden layer, and two internal and one external feedback loops exist to enhance the system estimation accuracy and convergence concurrently. The three-layers approximation is elaborated as follows:

1) *Input layer*. This layer is applied to monitor the input approximation error and obtains the feedback information from the output layer. The weight ϖ_5 of the neural network is used to combine the input layer with the output layer. By using the input vector e (i.e., e_1 and e_2), the outputs of this layer are

$$\varepsilon_l = \varpi_5 y_l + e_l, l = 1,2 \tag{42}$$

2) *Hidden layer*. By integrating the multiplication of the input signal, we obtain the output of this layer $r_k(N)$

$$r_k(N) = (1-\psi_k(N))\exp\left[-\theta_j^2(N)/2\right]\Pi_j(\theta_j(N)) + \psi_k(N) r_k(N-1) \tag{43}$$

where $\psi_k(N) \in (0,1)$ is the weight, Π_j and θ_j are defined by

$$\Pi_n(\theta_j) = \begin{cases} 1 & n=1 \\ 2\theta_j & n=2 \\ 2\theta_j \Pi_{n-1}(\theta_j) - 2(n-1)\Pi_{n-2}(\theta_j) & n \ge 3 \end{cases} \tag{44}$$

$$\theta_j(N) = \kappa_{1i}(N) \cdot \kappa_{2j}(N) \tag{45}$$

where κ_{1i} and κ_{2j}, $i = 1,..,5$, $j = 1,...,5$ are the outputs of the fuzzification process, which can be determined by

$$\kappa_{1i}(N) = c_{1i} \exp\left[-(\varepsilon_1 + \varpi_{3i}\kappa_{1i}(N-1) - a_{1i}^2)^2 \,|\, b_{1i} \,|^{-1}\right] \tag{46}$$

$$\kappa_{2j}(N) = c_{2j} \exp\left[-(\varepsilon_2 + \varpi_{4j}\kappa_{2j}(N-1) - a_{2j}^2)^2 \,|\, b_{2j} \,|^{-1}\right] \tag{47}$$

where ϖ_{3i} and ϖ_{4j} denote the internal feedback weight gains, $\varpi_1 = [a_{11},...,a_{15},a_{21},...,a_{25}]^{\mathrm{T}}$ denotes the center offset matrix, $\varpi_2 = [b_{11},...,b_{15},b_{21},...,b_{25}]^{\mathrm{T}}$ denotes the base width matrix, and c_{1i} and c_{2j} are positive weight constants.

3) *Output layer*. This layer calculates the output of the neural network under different system inputs. Then, the output can be fed back to the input layer through external loop. The weight w_k is used to link the output layer neurons and each neuron in the hidden layer. Specifically, the output $y(N)$ is specified as

$$y(N) = \sum_{k=1}^{25} w_k(N) r_k(N) = w_1(N) r_1(N) + \ldots + w_k(N) r_k(N) \tag{48}$$

where N is the iteration number, w_k is the weight between the hidden and output layers. With feedback gain ϖ_5, the output and input layers are connected, and the feedback signal can be fed back to the neurons of the input layer.

C. Stability Analysis

Theorem 2: If the proposed FST-SMC law determined by (36) is employed, then, the asymptotic stability of the decoupled FOMR system can be guaranteed.

Proof: We choose a Lyapunov function candidate as

$$V = V_1 + 0.5\Big[\sum_{i=1}^{2} \varsigma_i^{-1}(\sigma_i - \sigma_i^*)^2 + \tau_w^{-1} tr(\tilde{w}^T \tilde{w}) + \sum_{i=1}^{5} \tau_i^{-1} tr(\tilde{\varpi}_i^T \tilde{\varpi}_i) + s^{\mathrm{T}} s\Big] \tag{49}$$

where $\varsigma_{i=1,2}$, σ_i^*, τ_w and $\tau_{i=1,...,5}$ are positive constants.

By using $\mathrm{T} = V_1 + 0.5\sum_{i=1}^{2} \varsigma_i^{-1}(\sigma_i - \sigma_i^*)^2$, we have

$$\dot{V} = \dot{\mathrm{T}} + \sum_{i=1}^{5} \tau_i^{-1} tr(\tilde{\varpi}_i^{\mathrm{T}} \dot{\tilde{\varpi}}_i) + \tau_w^{-1} tr(\tilde{w}^{\mathrm{T}} \dot{\tilde{w}}) + s^{\mathrm{T}} \dot{s} \tag{50}$$

With $\tilde{\sigma}_i = \sigma_i - \sigma_i^*$ and positive constants $\Lambda_{i=1,2}$, we obtain

$$\begin{aligned} \dot{\mathrm{T}} &\le -\Upsilon V_1^{0.5} + \sum_{i=1}^{2} \varsigma_i^{-1} \tilde{\sigma}_i \dot{\sigma}_i \\ &\le -\Upsilon V_1^{0.5} + \sum_{i=1}^{2} \varsigma_i^{-1} \tilde{\sigma}_i \dot{\sigma}_i - \sum_{i=1}^{2} \frac{\Lambda_i}{\sqrt{2\varsigma_i}} |\tilde{\sigma}_i| + \sum_{i=1}^{2} \frac{\Lambda_i}{\sqrt{2\varsigma_i}} |\tilde{\sigma}_i| \end{aligned} \tag{51}$$

Define $\Upsilon_0 = \min(\Upsilon, \Lambda_1, \Lambda_2)$, it can be concluded that

$$-\Upsilon V_1^{0.5} - \sum_{i=1}^{2} \Lambda_i (2\varsigma_i)^{-0.5} |\tilde{\sigma}_i| \le -\Upsilon_0 \sqrt{\mathrm{T}} \tag{52}$$

Further, one can achieve

$$\dot{\mathrm{T}} \le -\Upsilon_0 \sqrt{\mathrm{T}} + \underbrace{\sum_{i=1}^{2} \varsigma_i^{-1} \tilde{\sigma}_i \dot{\sigma}_i + \sum_{i=1}^{2} \Lambda_i (2\varsigma_i)^{-0.5} |\tilde{\sigma}_i|}_{\Gamma} \tag{53}$$

Since there exists $\sigma_i^* > 0$ satisfying $\tilde{\sigma}_i < 0$, rewrite (53) as

$$\dot{\mathrm{T}} \le -\Upsilon_0 \sqrt{\mathrm{T}} - \sum_{i=1}^{2} |\tilde{\sigma}_i| (\varsigma_i^{-1} \dot{\sigma}_i - \Lambda_i (2\varsigma_i)^{-0.5}) \tag{54}$$

Thus, there exist the constants Λ_i and ς_i guaranteeing $\dot{\mathrm{T}} \le -\Upsilon_0 \sqrt{\mathrm{T}}$ (e.g., $\varsigma_i^{-1} \dot{\sigma}_i = \Lambda_i (2\varsigma_i)^{-0.5}$). This results in

$$\begin{aligned} \dot{V} &\le \dot{\mathrm{T}} + s^{\mathrm{T}} \Xi \left((\mathrm{G} - \hat{\mathrm{G}}) - \sigma_1 \Omega_1 - \sigma_2 \Omega_2 \right) \\ &+ \sum_{i=1}^{5} \tau_i^{-1} tr(\tilde{\varpi}_i^T \dot{\tilde{\varpi}}_i) + \tau_w^{-1} tr(\tilde{w}^{\mathrm{T}} \dot{\tilde{w}})) \\ &\le s^{\mathrm{T}} \Xi \left(\chi_m - \sigma_1 \Omega_1(s) - \sigma_2 \Omega_2(s) \right) + \tau_w^{-1} tr(\tilde{w}^{\mathrm{T}} \dot{\tilde{w}}) \\ &+ \sum_{i=1}^{5} \tau_i^{-1} tr(\tilde{\varpi}_i^{\mathrm{T}} \dot{\tilde{\varpi}}_i) + s^{\mathrm{T}} \Xi \left(\tilde{w}^{\mathrm{T}} (\hat{r} + \sum_{i=1}^{5} dr_{\varpi_i} \tilde{\varpi}_i) \right) \end{aligned} \tag{55}$$

By updating the learning parameters with $\dot{\tilde{w}} = -\tau_w s^{\mathrm{T}} \Xi \hat{r}$, $\dot{\tilde{\varpi}}_i = -\tau_i s^{\mathrm{T}} \Xi \tilde{w}^{\mathrm{T}} dr_{\varpi_i}, i = 1,...,5$, we can obtain

$$\begin{cases} s^{\mathrm{T}} \Xi \tilde{w}^{\mathrm{T}} \hat{r} + \tau_w^{-1} tr(\tilde{w}^{\mathrm{T}} \dot{\tilde{w}}) = 0 \\ s^{\mathrm{T}} \Xi \tilde{w}^{\mathrm{T}} \sum_{i=1}^{5} dr_{\varpi_i} \tilde{\varpi}_i + \sum_{i=1}^{5} \tau_i^{-1} tr(\tilde{\varpi}_i^{\mathrm{T}} \dot{\tilde{\varpi}}_i) = 0 \end{cases} \tag{56}$$

Then, one can reformulate (55) as

$$\begin{aligned} \dot{V} &\le s^{\mathrm{T}} \Xi \left(\chi_m - \sigma_1 \left(\zeta_1 \square s \square^{\alpha} + \zeta_2 \square s \square^{1/2} \right) - \sigma_2 \int \dot{\Omega}_2(s) dt \right) \\ &\le -\sigma_1 \Xi \left(\zeta_1 |s^{\mathrm{T}}||s|^{\alpha} + \zeta_2 |s^{\mathrm{T}}||s|^{0.5} \right) + |s|^{\mathrm{T}} \Xi |\chi_m| \\ &- \Xi \sigma_2 \int \left(\zeta_1^2 \alpha |s^{\mathrm{T}}||s|^{2\alpha-1} + (1+\alpha)|s^{\mathrm{T}}||s|^{\alpha-0.5} + 0.5\zeta_2^2 |s^{\mathrm{T}}| \right) dt \\ &= -\sigma_1 \Xi \left(\zeta_1 |s^{\mathrm{T}}||s|^{\alpha} + \zeta_2 |s^{\mathrm{T}}||s|^{0.5} \right) - \Xi |s^{\mathrm{T}}| \\ &\int \left(\sigma_2 \zeta_1^2 \alpha |s|^{2\alpha-1} + \sigma_2 (1+\alpha)|s|^{\alpha-0.5} + 0.5\sigma_2 \zeta_2^2 - |\dot{\chi}_m| \right) dt \\ &\le -\sigma_1 \Xi \left(\zeta_1 |s^{\mathrm{T}}||s|^{\alpha} + \zeta_2 |s^{\mathrm{T}}||s|^{0.5} \right) - \Xi |s^{\mathrm{T}}| \int \left(0.5\zeta_2^2 \sigma_2 - |\dot{\chi}_m| \right) dt \end{aligned} \tag{57}$$

Given that $\sigma_1 \Xi > 0$ and $|\dot{\chi}_m|$ is bounded, we have $\sigma_2 > 2\chi_d / \zeta_2^2$, leading to the following inequality

$$\dot{V} \le -\sigma_1 \Xi \left(\zeta_1 |s^{\mathrm{T}}| \cdot |s|^{\alpha} + \zeta_2 |s^{\mathrm{T}}| \cdot |s|^{0.5} \right) \le 0 \tag{58}$$

Note that (58) presents that $\dot{V} \le 0$ guarantees the asymptotic stability of the resultant FOMR system. Then, on the basis of the Barbalat Lemma [37], one can conclude that s will converge to zero as $t \to \infty$ and $\lim_{t \to \infty} e(t) = 0$. Combining Theorem 1, it is noted that the initial error and disturbances will affect the reaching time of the desired sliding manifold, but the

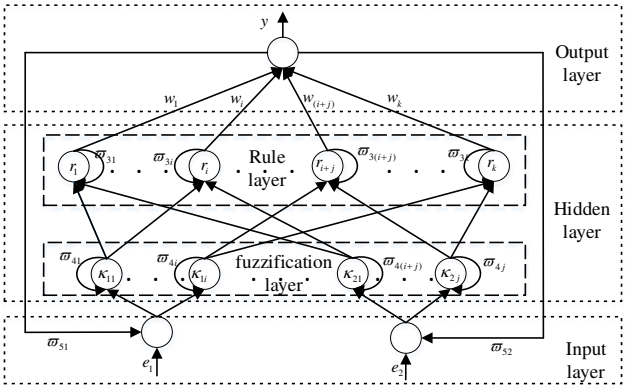

Fig. 3 Three-layer structure of the constructed MFNN

global convergence and stability can be maintained. Under the decoupling FST-SMC scheme, the FOMR system is stabilized under any initial conditions. This completes the proof. ■

IV. Comparison and Parameter Specifications

A. Comparison with Existing Methods

1) The characteristics of the considered terrain conditions that typically occur in industrial applications include: (1) The uneven ground will disarrange the driving or actuating forces of the FOMR, thus resulting in insufficient accuracy or even leading to unstable behaviors; and (2) Oiled terrain may cause wheel slip and lateral sway, failing to generate sufficient yaw moment. Given that the harsh terrain conditions will harm the system tracking performance or even results in unstable dynamics, this paper especially attempts to achieve a stable and accurate decoupled control of the FOMR, which ensures strong robustness against harsh terrain conditions in two ways: (1) With fractional super-twisting switching law, an enhanced FST-SMC is designed to ensure the nominal tracking performance without to gain overestimation or undesirable chattering (cf., [31], [35]); and (2) An MFNN-based unbiased fuzzy estimator is designed to actively compensate for the lumped disturbances, which differs from the traditional decoupling methods [23]. Given this context, the inevitable disturbances or uncertainties caused by nonideal modeling or linearization can be well addressed comprehensively.
2) For conventional SMC solutions, the discontinuous term ***sign***(*) is applied to construct the reaching law, thus forcing the controlled system states to the designed sliding mode manifold. The high frequency switching intrinsic property may lead to undesired oscillations. To alleviate the system tremor caused by the control method itself, the reaching law can be enhanced by (*i*) modifying ***sign*** with boundary layer methods, such as ***sat*** function or ***tanh*** function to smoothen the discontinuity occurring in the reaching law; (*ii*) or some integration of proportional and power rate terms [38], [39].
3) The following significant features of the derived multi-layer MFNN are worth noting: (1) Multiple loops (i.e., two inner and one external feedback loops) are considered, which can store more information to obtain improved approximation performance of the unknown disturbances; (2) Compared with the traditional neural network that has a fixed base width and center vector (such as [40]), these parameters can be scheduled in an online manner to achieve optimal values; (3) It can jointly prevent the system from oscillation caused by sudden changes of estimated disturbances to reach steady states. Thus, the FOMR system can track the desired trajectories to achieve superior control accuracy and robustness.

B. Parameter Determination

1) For practical application, the control parameter σ_1 should be selected on the basis of Theorem 1. This scheme does not consider the adaptive gain regulation or it may derive overestimated constant gains, leading to mitigated performance (in principle, one should adopt large control gains, however, this may subtract some unstable control responses). To accommodate this issue, we will adaptively schedule the control gains with the following rule: if $\sigma_1 \le \sigma_{\min}$ or $|s_1| \ge \omega_1$, $\dot{\sigma}_1 = \mu_1$, else $\dot{\sigma}_1 = -\mu_1$, where ω_1 and μ_1 are positive constants, and $\sigma_{\min}$ denotes the minimum of respective gains. To increase the anti-disturbance ability of the control system, one can make a trade-off between disturbances mitigation and dynamic tracking. If the tracking error increases, the control gains will increase to enhance the profile following capacity; however, if the tracking error is relatively smaller, we prefer smaller gains to maintain the system control stability. Through the adaptive adjustment of gain, the ability of anti-disturbance is increased, and the system instability caused by excessive gain is avoided.
2) The integral sliding surfaces can be achieved by specifying $\alpha, \rho \in (0,1)$ [41], [42]. A distinguishing feature is that the finite reaching time of the desired sliding manifold can be regulated flexibly on the basis of (34) and (35). In practice, real-time regulation of α and ρ may improve the lateral tracking performance, but the increased calculation burden cannot be ignored. Meanwhile, the fractional calculus can be approximated by fractional order differences and *n*-iteration-steps-sums in microprocessor computations, which is suitable for a practical FSMR application [14]. The fractional orders are pre-tuned, and the order *n* is specified as 5 to make the tradeoff of computation burden and control efficiency.
3) A singularity issue may occur for the term $e^{\eta_1/\eta_2 - 1}\dot{e}$ in traditional terminal SMC designs [43], [44]. This implies that a bounded control effect cannot be guaranteed if $\dot{e} \ne 0$ when $e = 0$. For the derived control law, η_1 and η_2 are ensured to be positive odd numbers here satisfying $1 < \eta_1/\eta_2 < 2$. Therefore, the singularity problem of the traditional terminal SMC can be overcome completely.

V. Experimental Verifications

A. Experimental setup

For practical implementation, Fig. 4 shows the FOMR platform and experimental scenario in a real manufacturing factory. The experiment environment is interfaced with unsatisfactory ground conditions, such as road damage, oil/water mixing ground, and other complex external disturbances. This process is normal in a typical manufacturing factory, which may lead to wheel slip and lateral sway due to the reduced friction and tire deformation. It provides a real-life

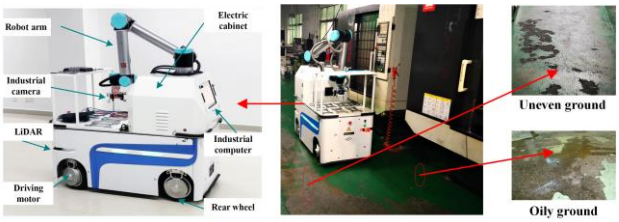

Fig. 4 Developed platform and experimental scenario

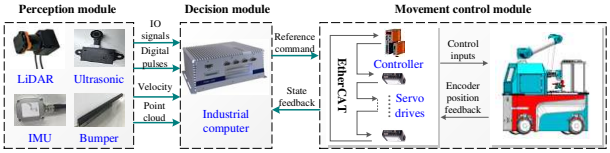

Fig. 5 Hardware information of FOMR system

TABLE 1. SPECIFICATIONS OF THE DEVELOPED SYSTEM

Parameters	Values	Parameters	Values
Length	0.96 m	Yaw moment of inertia	130 kgm^2
Width	0.53 m	Robot width	0.56 m
Main frequency of PC	2.59 GHz	Total	1000 kg
RAM of PC	8 G	Duration time	8 h
Encoder	2500 ppr	Max speed	1.5 m/s

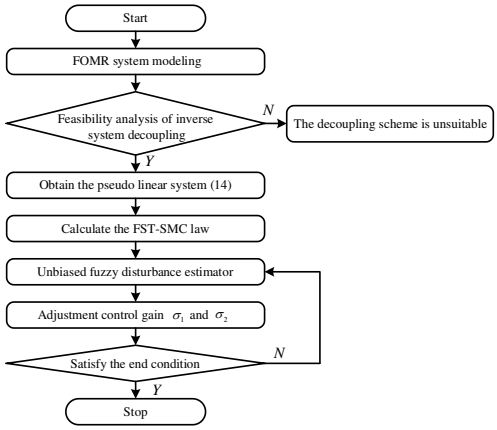

Fig. 6 Implementation procedure of the proposed scheme

scenario to verify the anti-disturbance ability of our method under harsh terrain conditions. The specific hardware structure is shown in **Error! Reference source not found.**, which comprises: (*i*) Perception layer: The layer uses various installed sensors to obtain the detected data, and realizes environment detection, map construction, and state feedback; (*ii*) Decision layer: This module uses the collected data and information to help FOMR make the best response to ensure the safe, efficient and high-precision operation of the system; (*iii*) Actuation layer: By receiving the data of the decision layer, the operation mode is configured efficiently, and the control law issued by the decision layer is completed to realize the smooth operation of FOMR.

The specific experimental process is shown in Fig. 6, which mainly includes parameter initialization, model decoupling, disturbance estimation, control law calculation, and gain regulation. The system specifications are determined by TABLE 1. In correspondence with the analyses on *Section IV(B)*, the control parameters are selected as $\eta_1 = 5$, $\eta_2 = 3$, $\alpha = \rho = 0.9$, $\zeta_1 = \zeta_2 = 1$, $\lambda = diag\{2,1\}$, $\sigma_{\min} = [0.18, 0.3]^{\mathrm{T}}$, $\omega_1 = [0.0017, 0.002]^{\mathrm{T}}$, $\tau = [1,1]^{\mathrm{T}}$, $\mu_1 = [0.01, 0.01]^{\mathrm{T}}$, $\tau_w = 3\times10^5$, $\tau_{i=1,\ldots,5} = 1\times10^4$, $w = diag\{0.1176, 0.1176\}$. It should be mentioned that these related parameters can be tuned by some adaptive methods [44].

B. Inverse System Decoupling Results

In this subsection, the decoupling features of the proposed asymptotic stabilization scheme are identified. To this end, a pulse signal is used to excite the constituted decoupled system. As shown in Fig. 7, a sudden change of one reference input minimally influences the other output. That is, when u_1 is activated, β changes correspondingly, but γ has a slight vibration. Meanwhile, when u_2 is excited, γ will change, whereas β has no obvious change. Although the form of the inverse system can be close to the actual mathematical model of the FOMR system, there inevitably exist modeling errors and unmodeled dynamics. This leads to subtle fluctuations among variables and decoupling oscillations, as can be seen from the enlarged γ in Fig. 7(a) and the enlarged β in Fig. 7(b). This will be further accommodated by the designed disturbance estimator. Thus, the proposed method realizes the decoupling of yaw rate β and sideslip angle γ, and ensures the independent control of the lateral motion states, i.e., β and γ.

C. Lateral Tracking Results

In this section, two cases are used to verify the lateral tracking performance and robustness of the proposed control strategy. The traditional terminal SMC (TSMC) and decoupling TMSC (DTSMC) methods without fuzzy disturbances estimator are selected to compare to our FST-SMC method. A fair comparison can be ensured given that (*i*) All the comparison controllers are pre-tuned optimally under the chattering-free design scheme with the same initial state and control parameters of the FOMR, and (*ii*) The experiments are performed under the same operating conditions.

Case 1): The widely employed Ackerman mode is applied here. The yaw rate tracking results and related following errors are shown in Fig. 8(*a*) and Fig. 8(*b*), respectively. Fig. 8 exhibits that the traditional methods and our proposed FST-SMC schemes can achieve stable lateral tracing control. Fig. 8(*b*) presents that the following errors of the TSMC control scheme will lead to larger vibrations due to the lumped disturbances and uncertainties. In comparison, the presented decoupling FST-SMC obtains enhanced precision and smoother states. For example, there exist overshoots with magnitudes of 0.01774 rad/s and 0.01288 rad/s under the comparative TSMC and DTSMC methods, respectively. The proposed decoupling FST-SMC scheme can mitigate these undesired overshoots, yielding a satisfactory yaw rate tracking control during the whole control process. As shown in Fig. 9, the similarity results can be found in the sideslip angle tracking responses. Subjecting to unsatisfactory terrain conditions, one can observe numerous vibration changes with tremendous peaks in the traditional TSMC control systems. Compared with our presented method, the conventional TSMC and the DTSMC schemes will lead to non-ignorable overshoots. Our presented anti-disturbance FST-SMC scheme provides more dynamical robustness to make resultant trajectories being closed to the reference ones. Specifically, a steady decrease exists in the error peaks from over 0.007412 rad (under TSMC method) or 0.004357 rad (under DTSMC method) to around 0.002945 rad (under our proposed method).

Fig. 10 shows the relating signals, including yaw moment and steering angle, while Fig. 11 shows the control gain and

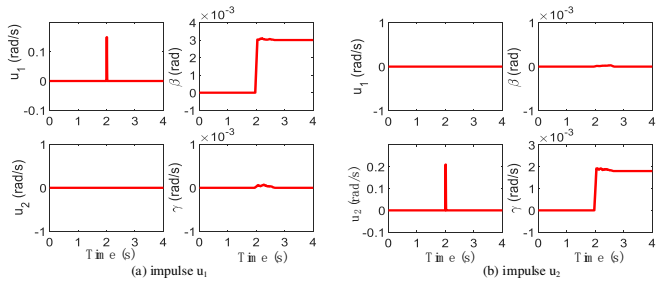

Fig. 7 System response under the decoupling control

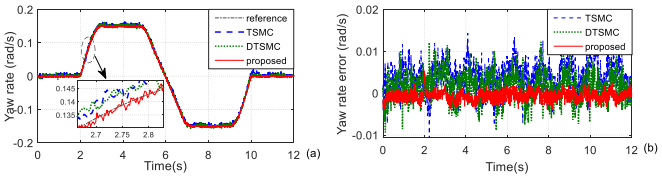

Fig. 8 Yaw rate responses in case 1

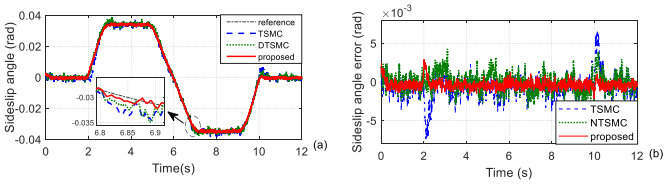

Fig. 9 Sideslip angle responses in case 2

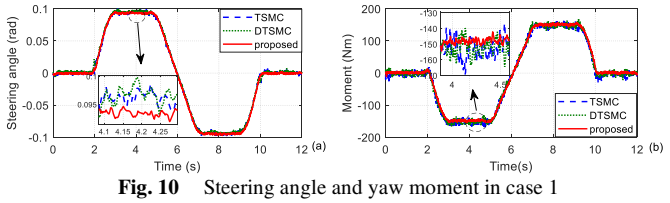

Fig. 10 Steering angle and yaw moment in case 1

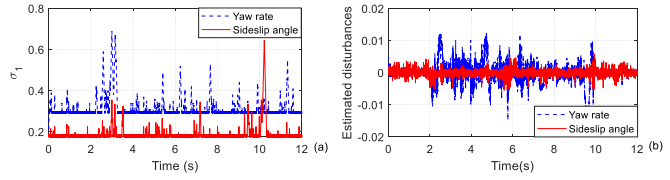

Fig. 11 Gain of σ_1 and the estimated disturbances in case 1

estimated disturbances. The adaptive variable gains are beneficial for restraining the lumped disturbances efficaciously. Thus, it can be applied to automatically and adaptively regulate the controller to various operating conditions. For a clearer quantitative illustration, the performance criteria in terms of max, average, and integral standard deviation (ISD) of the corresponding lateral tracking errors are specifically provided in TABLE 2. Overall, owing to our presented FST-SMC law, one can achieve optimal features concerning smoother response and smaller dynamic errors, thus enhancing the lateral motion stabilization performance of the considered FOMR system.

Further, to evaluate the time-delay effect for MLNN-based disturbance estimation, the time assumed is compared by

TABLE 2. CRITERIA UNDER THE COMPARISON CONTROLLERS IN CASE 1

States	Methods	Criteria (10^{-4})		
		Max	Average	ISD
Yaw rate	TSMC	177.74	40.67	28.69
	DTSMC	128.82	28.32	20.54
	proposed	53.13	10.36	7.78
Sideslip angle	TSMC	74.12	12.00	11.75
	DTSMC	43.57	9.22	7.19
	proposed	29.45	5.33	3.83

TABLE 3. CONSUMING TIME OF THE COMPARISON METHODS IN CASE 1

Methods	Max (ms)	Average (ms)	STD
DTSMC	43	21.1961	2.8509
TSMC	41	21.1070	2.8311
Proposed	44	23.1379	3.0750

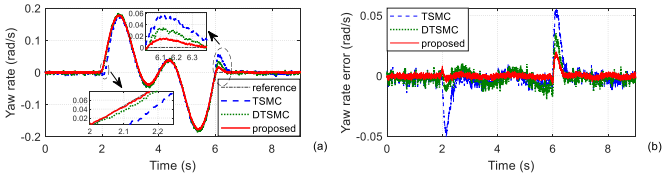

Fig. 12 Yaw rate response in case 2

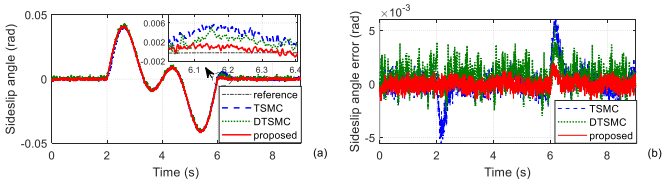

Fig. 13 Sideslip angle response in case 2

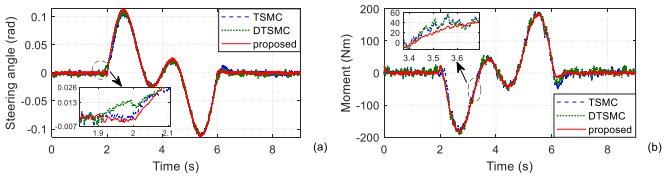

Fig. 14 Steering angle and yaw moment in case 2

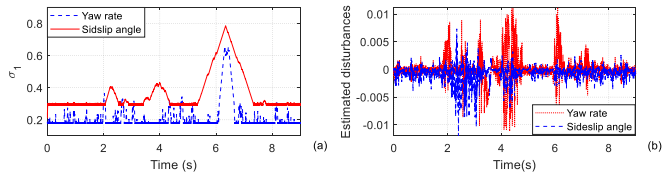

Fig. 15 Gain of σ_1 and the estimated disturbances in case 2

TABLE 4. CRITERIA UNDER THE COMPARISON CONTROLLERS IN CASE 2

States	Methods	Criteria (10^{-4})		
		Max	Average	ISD
Yaw rate	TSMC	560.27	63.01	95.83
	DTSMC	350.69	45.27	46.66
	proposed	157.58	15.32	23.01
Sideslip angle	TSMC	56.05	6.37	9.64
	DTSMC	35.10	4.52	4.72
	proposed	15.85	1.50	2.36

performing 100 times experiments. The results are shown in TABLE 3. To eliminate the accidental error, the maximum, average, and standard deviation (STD) values are selected for analysis. Taking the average value as an example, the proposed method consumes roughly 2 ms more time than DTSMC and TSMC, which can be ignored for an industrial practical implementation. Therefore, the time-delay effect caused by an unbiased fuzzy disturbance estimator will not affect the real-time implementation of the proposed FST-SMC method.

Case 2): In this case, with the continuous sinusoidal desired signal, the lateral tracking performance of the comparison method is tested under unsatisfactory ground conditions. Fig. 12 and Fig. 13 demonstrate the dynamic tracking responses of yaw rate and sideslip angle, respectively. These figures present that the comparison methods can achieve stable resultant responses. Compared with traditional methods, the proposed decoupling FST-SMC method has the smallest overshoot at the smooth corner and less jitter during tracking control. Take the yaw rate for example. As shown in Fig. 13, the overshoot under the TSMC method has an amplitude of 0.005602 rad and the

integrated method can achieve a smaller overshoot with a maximum error of 0.001575 rad. The overshoot is reduced up to 80.2191 %. This signifies that the decoupled FOMR system keeps the tracking responses close to the required responses and strengthens the system's robustness.

For the proposed decoupling FST-SMC method, the steering angle and yaw moment are shown in Fig. 14, and the vibration tendency of σ_1 and the estimated disturbances are shown in Fig. 15. These results show that our method can offer smoother responses and improved stability for the FOMR system as a benefit of its adaptively regulated control law. Further, the quantified criteria in terms of max, average and ISD of the absolute tracking errors are provided in TABLE 4, which shows improved robustness of our presented method.

Among the comparison methods, the proposed one can converge to a steady-state with the lowest tracking errors. This provides evidence that the presented decoupling FST-SMC method can ensure the optimal lateral stabilization control performance for the concerned FOMR system when applying to a harsh environment with uneven and oiled terrain.

VI. Conclusion

In this paper, a decoupled FST-SMC method was proposed to stabilize the interconnected FOMR system under harsh terrain conditions. An inverse system-based decoupling method was integrated into the FST-SMC framework to transfer the original interconnected system into an integral pseudo linear composition system. A novel FST-SMC nominal regulation law was proposed to drive the closed-loop states into a bounded region. The adaption of the MFNN gains leads to a system that is insensitive to unknown disturbances. Theoretical analyses were conducted to ensure the asymptotic convergence, the anti-disturbance feature, and the closed-loop stability of the achieved decoupled system. Comparative experiment results verified the practicability and superiorities of the asymptotic decoupling stabilization control in two operating conditions.

In this paper, the time delay issue is not the main concern given that this paper focused on the anti-disturbance decoupling control of interconnected FOMR systems. However, in a highly disturbed environment, the hybrid time-varying delays or packet dropouts exist in the sampler-to-control station and the control station-to-actuator communication network channels. This might lead to system instability under a networked control scheme if not well handled. Given this context, the robust control of time-delayed FOMR systems will be explored in our future work to enhance the trajectory-tracking performance.

References

[1] P. Panahandeh, K. Alipour, B. Tarvirdizadeh, and A. Hadi, "A kinematic Lyapunov-based controller to posture stabilization of wheeled mobile robots," *Mechanical Syst. Signal Proce.*, vol.134, pp. 106319, 2019.

[2] D. Rotondo, V. Puig, F. Nejjari, and J. Romera, "A Fault-Hiding Approach for the Switching Quasi-LPV Fault-Tolerant Control of a Four-Wheeled Omnidirectional Mobile Robot," *IEEE Trans. Ind. Electron.*, vol. 62, no. 6, pp. 3932-3944, June 2015.

[3] J. Meng, *et al.*, "Iterative-learning error compensation for autonomous parking of mobile manipulator in harsh industrial environment," *Robot. Comput. Integr. Manuf.*, vol. 68, pp. 102077, 2020.

[4] C. Ren, X. Li, X. Yang, and S. Ma, "Extended state observer-based sliding mode control of an omnidirectional mobile robot with friction compensation," *IEEE Trans. Ind. Electron.*, vol. 6, no.12, pp. 9480-9489, Jan. 2019.

[5] J. Fu, *et al.*, "Motion tracking control design for a class of nonholonomic mobile robot systems," *IEEE Trans. Syst., Man, Cybern., Syst.*, vol. 50, no. 6, pp. 2150-2156, Mar. 2018.

[6] Z. Wang, U. Montanaro, S. Fallah, A. Sorniotti, and B. Lenzo, "A gain scheduled robust linear quadratic regulator for vehicle direct yaw moment control," *Mechatronics*, vol. 51, pp. 31-45, 2018.

[7] J. C. Wang, R. He, and Y. B. Kim, "Optimal anti-lock braking control with nonlinear variable voltage charging scheme for an electric vehicle," *IEEE Trans. Veh. Technon.*, vol. 69, no. 7, pp. 7211-7222, July 2020.

[8] C. H. Yang, C. Yang, T. Peng, X. Yang, and W. Gui, "A fault-injection strategy for traction drive control systems," *IEEE Trans. Ind. Electron.*, vol. 64, no. 7, pp. 5719-5727, Feb. 2017.

[9] N. Ahmadian, A. Khosravi, and Sarhadi P, "Integrated model reference adaptive control to coordinate active front steering and direct yaw moment control," *ISA Trans.*, vol. 106, pp. 85-96, 2020.

[10] S. Ding, L. Liu, and W. X. Zheng, "Sliding mode direct yaw-moment control design for in-wheel electric vehicles," *IEEE Trans. Ind. Electron.*, vol. 64, no. 8, pp. 6752-6762, Mar. 2017.

[11] J. S. Hu, Y. Wang, H. Fujimoto, and Y. Hori, "Robust yaw stability control for in-wheel motor electric vehicles," *IEEE/ASME Trans. Mechatron.*, vol. 22, no. 3, pp. 1360-1370, Mar. 2017.

[12] W. Zhao, H. Zhang, and Y. Li, "Displacement and force coupling control design for automotive active front steering system," *Mechanical Syst. Signal Proce.*, vol. 106, pp. 76-93, 2018.

[13] J. Ni, J. Hu, and C. Xiang, "Robust control in diagonal move steer mode and experiment on an X-by-wire UGV," *IEEE/ASME Trans. Mechatron.*, vol. 24, no. 2, pp. 572-584, Jan. 2019.

[14] Y. L. Xie, *et al.*, "Coupled fractional-order sliding mode control and obstacle avoidance of a four-wheeled steerable mobile robot," *ISA Trans.*, vol. 108, pp. 282-294, 2021.

[15] Y. Luo, T. Chen, and K. Li, "Multi-objective decoupling algorithm for active distance control of intelligent hybrid electric vehicle," *Mechanical Syst. Signal Proce.*, vol. 64, pp. 29-45, 2015.

[16] J. Lan and R. J. Patton, "A decoupling approach to integrated fault-tolerant control for linear systems with unmatched non-differentiable faults," *Automatica*, vol. 89, pp. 290-299, 2018.

[17] X. Sun, *et al.*, "High-performance control for a bearingless permanent-magnet synchronous motor using neural network inverse scheme plus internal model controllers," *IEEE Trans. Ind. Electron.*, vol. 63, no. 6, pp. 3479-3488, June 2016.

[18] W. Sun, J. W. Lin, S. F. Su, N. Wang, and M. J. Er, "Reduced Adaptive Fuzzy Decoupling Control for Lower Limb Exoskeleton," *IEEE Trans. Cybern.*, vol. 51, no. 3, pp. 1099-1109, Mar. 2021.

[19] H. Zhang and W. Zhao, "Decoupling control of steering and driving system for in-wheel-motor-drive electric vehicle," *Mechanical Syst. Signal Proce.*, vol.101, pp. 389-404, 2018.

[20] C. Wang, W. Zhao, Z. Luan, Q. Gao, and K. Deng, "Decoupling control of vehicle chassis system based on neural network inverse system," *Mechanical Syst. Signal Proce.*, vol. 106, pp. 176-197, 2018.

[21] R. Marino and S. Scalzi, "Asymptotic sideslip angle and yaw rate decoupling control in four-wheel steering vehicles," *Vehicle Syst. Dyn.*, vol. 48, no. 9, pp. 999-1019, 2010.

[22] L. Jiang, *et al.*, "Inverse Decoupling-based Direct Yaw Moment Control of a Four-wheel Independent Steering Mobile Robot," *In: Proc. of 2020 IEEE/ASME Int. Conf. Advanced Intel. Mechatron. (AIM), Boston, USA*, pp. 892-897, 2020.

[23] H. Shi, M. Xu and K. -S. Hwang, "A Fuzzy Adaptive Approach to Decoupled Visual Servoing for a Wheeled Mobile Robot," *IEEE Trans. Fuzzy Syst.*, vol. 28, no. 12, pp. 3229-3243, Dec. 2020.

[24] M. Li, C. Mao, Y. Zhu, K. Yang, and X. Li, "Data-Based Iterative Dynamic Decoupling Control for Precision MIMO Motion Systems," *IEEE Trans. Ind. Inf.*, vol. 16, no. 3, pp. 1668-1676, Mar. 2020.

[25] H. Zhou and H. Deng, "Hybrid fuzzy decoupling control for a precision maglev motion system," *IEEE/ASME Trans. Mechatron.*, vol. 23, no.1, pp. 389-401, Nov. 2017.

[26] Y. Fu, C. Hong, and J. Li, "Optimal decoupling control method and its application to a ball mill coal-pulverizing system," *IEEE/CAA J. Automatica Sinica*, vol. 5, no. 6, pp. 1035-1043, Aug. 2018.

[27] K. Shi, X. Yuan, G. Huang and Z. Liu, "Compensation-Based Robust Decoupling Control System for the Lateral and Longitudinal Stability of Distributed Drive Electric Vehicle," *IEEE/ASME Trans. Mechatron.*, vol. 24, no. 6, pp. 2768-2778, Dec. 2019.

[28] Y. Y. Wang, S. Jiang, Chen B, and H. Wu, "A new continuous fractional-order nonsingular terminal sliding mode control for cable-driven manipulators," *Adv. Eng. Soft.*, vol. 119, pp. 21-29, 2018.

[29] S. Jeong and D. Chwa, "Sliding-Mode-Disturbance-Observer-Based Robust Tracking Control for Omnidirectional Mobile Robots with Kinematic and Dynamic Uncertainties," *IEEE/ASME Trans. Mechatron.*, vol. 26, no. 2, pp. 741-752, Apr. 2020.

[30] J. Fei and Z. Feng, "Fractional-order finite-time super-twisting sliding mode control of micro gyroscope based on double-loop fuzzy neural network," *IEEE Trans. Syst., Man, Cybern., Syst.*, published online, doi:

10.1109/TSMC.2020.2979979, 2020.
[31] L. Jiang, *et al.*, "Anti-Disturbance Direct Yaw Moment Control of a Four-Wheeled Autonomous Mobile Robot," *IEEE Access*, vol. 8, pp. 174654-174666, Sep. 2020.
[32] K. Yong, M. Chen, and Q. Wu, "Anti-disturbance control for nonlinear systems based on interval observer," *IEEE Trans. Ind. Electron.*, vol. 67, no. 2, pp. 1261-1269, Feb. 2019.
[33] W. H. Chen, J. Yang, L. Guo, and S. Li, "Disturbance-observer-based control and related methods-An overview," *IEEE Trans. Ind. Electron.*, vol. 63, no. 2, pp. 1083-1095, Feb. 2015.
[34] Y. Yi, W. X. Zheng, and B. Liu, "Adaptive anti-disturbance control for systems with saturating input via dynamic neural network disturbance modelling," *IEEE Trans. Cybern.*, published online, doi: 10.1109/TCYB.2020.3029889, 2020.
[35] Y. Y. Wang, K. Zhu, F. Yan, and B. Chen, "Adaptive super-twisting nonsingular fast terminal sliding mode control for cable-driven manipulators using time-delay estimation," *Adv. Eng. Soft.*, vol. 128, pp. 113-124, 2019.
[36] Y. L. Xie, *et al.*, "Iterative Data-Driven Fractional Model Reference Control of Industrial Robot for Repetitive Precise Speed Tracking," *IEEE/ASME Trans. Mechatron.*, vol. 24, no. 3, pp. 1041-1053, June 2019.
[37] Z. Wu, Y. Xia, and X. Xie, "Stochastic Barbalat's Lemma and Its Applications," *IEEE Trans. Autom. Control*, vol. 57, no. 6, pp. 1537-1543, June 2012.
[38] S. M. Mozayan, M. Saad, H. Vahedi, H. Fortin-Blanchette, and M. Soltani, "Sliding Mode Control of PMSG Wind Turbine Based on Enhanced Exponential Reaching Law," *IEEE Trans. Ind. Electron.*, vol. 63, no. 10, pp. 6148-6159, Oct. 2016.
[39] T. Gonzalez, J. A. Moreno, and L. Fridman, "Variable Gain Super-Twisting Sliding Mode Control," *IEEE Trans. Autom. Control*, vol. 57, no. 8, pp. 2100-2105, Aug. 2012.
[40] Z. Chen, F. Huang, W. Sun, J. Gu, and B. Yao, "RBF-Neural-Network-Based Adaptive Robust Control for Nonlinear Bilateral Teleoperation Manipulators With Uncertainty and Time Delay," *IEEE/ASME Trans. Mechatron.*, vol. 25, no. 2, pp. 906-918, April 2020.
[41] Y. L. Xie, X. Q. Tang, B. Song, X. D. Zhou, and Y. X. Guo, "Data-driven adaptive fractional order PI control for PMSM servo system with measurement noise and data dropouts," *ISA Trans.*, vol. 75, pp. 172-188, 2018.
[42] B. T. Zhang, Y. G. Pi, and Y. Luo, "Fractional order sliding-mode control based on parameters auto-tuning for velocity control of permanent magnet synchronous motor," *ISA Trans.*, vol. 51, no. 5, pp. 649-656. 2012.
[43] S. Chen and F. Lin, "Robust Nonsingular Terminal Sliding-Mode Control for Nonlinear Magnetic Bearing System," *IEEE Trans. Control Syst. Technon.*, vol. 19, no. 3, pp. 636-643, May 2011.
[44] S. S. Xu, C. Chen, and Z. Wu, "Study of Nonsingular Fast Terminal Sliding-Mode Fault-Tolerant Control," *IEEE Trans. Ind. Electron.*, vol. 62, no. 6, pp. 3906-3913, June 2015.

Liquan Jiang received the B.S. degree in mechanical engineering from China University of Geosciences, Wuhan, China, in 2014, the M.S. degree in mechanical and Electronic Engineering from Huazhong University of Science and Technology (HUST), Wuhan, China, in 2017.

He is currently pursuing the Ph.D. degree with the School of Mechanical Science and Engineering, HUST, China. His research interests include robot control and path planning.

Shuting Wang received the B.S. and M.S. degrees from the school of energy and power engineering, Wuhan University of Technology, Wuhan, China, in 1991 and 1994, respectively, and the Ph.D. degree from the School of Mechanical Science and Engineering, Huazhong University of Science and Technology (HUST), Wuhan, China, 2002.

He is currently a full professor and Vice-president with the School of Mechanical Science and Engineering of HUST. He has published more than 90 articles. His research interests include mobile robot, mechanical design, and numerical control.

Yuanlong Xie received his B.S. degree in electrical engineering and Ph.D. degree in mechanical engineering from Huazhong University of Science and Technology (HUST), Wuhan, China, in 2014 and 2018, respectively.

He was an Academic Visitor with the School of Electronic and Electrical Engineering, University of Leeds, Leeds, U.K., from 2017 to 2018. He has been a Postdoctoral Fellow with HUST from Nov. 2018. He has published more than 60 academic journal and conference papers. His research interests include robot control and servo control.

Shengquan Xie (SM'11) received the Ph.D. degrees in mechatronics engineering from Huazhong University of Science and Technology, Wuhan, China and in mechanical engineering from the University of Canterbury, Christchurch, New Zealand, in 1998 and 2002, respectively.

In 2003, he joined the University of Auckland and became a Chair Professor of (Bio) Mechatronics in 2011. Since 2017, he has been the Chair Professor of Robotics and Autonomous Systems with the University of Leeds, Leeds, U.K. He has authored or coauthored 8 books, 15 book chapters, and more than 400 international journal and conference papers. His research interests include medical and rehabilitation robots and advanced robot control. Prof. Xie is an elected Fellow of The Institution of Professional Engineers New Zealand (FIPENZ). He has also served as a Technical Editor for *IEEE/ASME TRANSACTIONS ON MECHATRONICS*.

Shiqi Zheng received the Ph.D. degree from the school of Mechanical Science and Engineering, Huazhong University of Science and Technology, Wuhan, China, in 2016.

He was an Academic Visitor with the School of Electrical and Electronic Engineering, The University of Adelaide, Adelaide, Australia, from 2018 to 2019. He is currently a Professor with the China University of Geosciences, Wuhan. His current research interests include switched control and multiagent systems.

Jie Meng received the B.S. degrees in mechanical engineering from Wuhan Universi- ty of Technology, Wuhan, China, in 2016.

He is currently pursuing the Ph.D. degree with the School of Mechanical Science and Engineering, Huazhong University of Science and Technology, Wuhan, China. He has published 4 academic journal and conference papers, and hold 2 patents. His research interests include robot perception and mobile robot navigation.

Han Ding (Senior Member, IEEE) received the Ph.D. degree in mechanical engineering from the Huazhong University of Science and Technology (HUST), Wuhan, China, in 1989. From 1993 to 1994, he was with the University of Stuttgart, Stuttgart, Germany, supported by the Alexander von Humboldt Foundation. Since 1997, he has been a Professor with HUST, where he is currently the Director of the State Key Lab of Digital Manufacturing Equipment and Technology. From 2001 to 2006, he was a Cheung Kong Chair Professor with Shanghai Jiao Tong University, Shanghai, China. His research interests include robotics and multiaxis machining.

Dr. Ding is an Editor for the *IEEE TRANSACTIONS ON AUTOMATION SCIENCE AND ENGINEERING* and a Senior Editor for the *IEEE ROBOTICS AND AUTOMATION LETTERS*. He was elected as a Member of the Chinese Academy of Sciences, in 2013.